Integration of shape information occurs around closed contours but not across them

Robert J. Green School of Psychological Science, The University of Western Australia, Perth, Australia

J. Edwin Dickinson School of Psychological Science, The University of Western Australia, Perth, Australia

David R. Badcock School of Psychological Science, The University of Western Australia, Perth, Australia

Scenery and complex objects can be reduced to a combination of shapes, so it is pertinent to examine if the integration of information found occurring around simple contours also occurs across them. Baldwin, Schmidtmann, Kingdom, and Hess (2016) investigated this idea using radial frequency (RF) patterns, distributing information around a single contour or across four contours. However, their use of a restricted number of locations for this information may have influenced their results (see Green, Dickinson, & Badcock, 2017). The current study revisits their paradigm using random-phase (spatial uncertainty) presentation of RF patterns with 11 observers. Results provide strong evidence for the integration of information around single contours but not across them. These findings are contrary to the lack of integration found by Baldwin et al. (2016) within a single contour, but do provide support for their suggestion that improvement in performance when adding information to separate RF patterns is a function of probability summation. Similar to Green et al. (2017), it suggests the importance of using random-phase RF patterns when measuring integration.

Introduction

The human visual system decodes the image presented to find appropriately arranged elements that may indicate the presence of an object. This is thought to occur through the combination of local orientation and corners (Dickinson, Cribb, Riddell, & Badcock, 2015; Persike & Meinhardt, 2017) into more complex objects (faces, houses, etc.) and scenes (Van Essen, Anderson, & Felleman, 1992; Vernon, Gouws, Lawrence, Wade, & Morland, 2016). Spatial integration of adjacent local information can result in better sensitivities than predicted by the increased likelihood of detection that could arise simply from having more numerous local elements and has been used as one type of evidence of global processing. This integration has been shown to occur around both contours (Bell & Badcock, 2008; Cribb, Badcock, Maybery, & Badcock, 2016; Dickinson, McGinty, Webster, & Badcock, 2012; Hess, Wang, & Dakin, 1999; Loffler, Wilson, & Wilkinson, 2003; Tan, Dickinson, & Badcock, 2013) and textures (Tan, Bowden, Dickinson, & Badcock, 2015).

Radial frequency (RF) patterns (Wilkinson, Wilson, & Habak, 1998) have previously been used to examine the global processing of shapes. These patterns are circles that have had their radius sinusoidally modulated as a function of polar angle, and they are, therefore, closed contours that can be varied in shape (see Figure 1) to mimic the bounding contours of some objects, making them a useful stimulus in the study of shape perception. They are defined by their RF number (number of wavelengths able to fit in 360°) and the number of complete sinusoidal cycles actually present in the pattern. Increasing the amplitude of the modulating sine wave increases the pattern's deformation from circular and, therefore, increases the probability of the observer discriminating the RF pattern from a circle.

One method used for determining the presence of global processing in RF patterns is the comparison of the rate of reduction in observer thresholds, arising from increasing numbers of cycles of modulation of a fixed wavelength on the contour to the rate that would be predicted by probability summation. Probability summation is the increased chance of detection due to an increase in the number of local signals available on the contour, a number that increases as more cycles are

Citation: Green, R. J., Dickinson, J. E., & Badcock, D. R. (2018). Integration of shape information occurs around closed contours but not across them. *Journal of Vision*, *18*(5):6, 1–13, https://doi.org/10.1167/18.5.6.

https://doi.org/10.1167/18.5.6 Received September 18, 2017; published May 4, 2018 ISSN 1534-7362

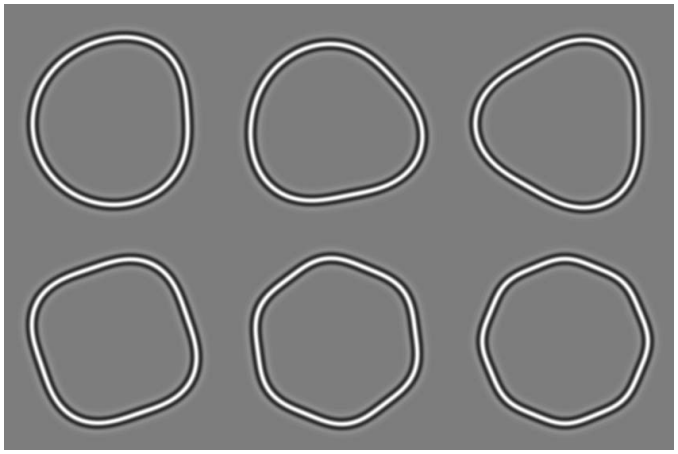

Figure 1. Example RF patterns. Top, left to right: an RF3(1), RF3(2), and RF3(3) (RF3 with one, two, and three cycles of modulation, respectively); bottom, left to right: an RF4, RF6, and RF8. All patterns have an amplitude of $1/(1+\omega^2)$, where ω is the RF number and results in a pattern well above threshold levels but shown for clarity.

added. However, the way in which probability summation was previously calculated has been called into question and is discussed below.

Complex scenes are made up of collections of objects, which can be further reduced to simple shapes and, in turn, local elements. Researchers have demonstrated the pooling of discrete local elements in a wide range of contexts, including dot pairs (Badcock, Clifford, & Khuu, 2005; Dickinson & Badcock, 2007; Dickinson, Broderick, & Badcock, 2009; Glass, 1969; Glass & Pérez, 1973; Morrone, Burr, & Vaina, 1995), Gabor patches (Dickinson, Han, Bell, & Badcock, 2010; Holmes & Meese, 2004; Tan et al., 2015), and both static (Baker & Meese, 2011; Meese, 2010; Meese & Hess, 2007) and moving gratings (McDougall, Dickinson, & Badcock, 2016). There is also evidence for the visual system's ability to extract group statistics from low-level visual elements (Ariely, 2001; Burr & Ross, 2008) and more complex scenes, such as determining the average emotion, gender, and identity from a crowd of faces (de Fockert & Wolfenstein, 2009; Haberman & Whitney, 2007; Haberman & Whitney, 2009). Considering this evidence, we might expect information from simple shapes, particularly those with shared parameters, to be pooled together across a surface by the visual system in a process similar to that used with local elements or a crowd of faces.

Baldwin, Schmidtmann, Kingdom, and Hess (2016) investigated the integration of information in two contexts. First, when the information was spread around a single contour of an RF pattern (within) and, second, when the same amount of modulation was applied to more than one contour (across). They used four RF4 patterns in a diamond arrangement (quad-RF condition) to examine detection thresholds across RF patterns and compared these results with detection thresholds within a pattern (single-RF condition). In their analysis, they determined there was little difference in the summation across RF patterns compared with within RF patterns, a result consistent with detection of local features rather than global integration of information around contours. Furthermore, they found no evidence to reject probability summation, which is indicative of local feature detection, and therefore, they found no evidence of global processing either within or across the RF4s when assessed using their method.

Baldwin et al. (2016) were unable to reject probability summation within RF patterns, a finding that is contrary to the conclusions of previous studies looking at integration of RF4 patterns (Dickinson et al., 2012; Schmidtmann, Kennedy, Orbach, & Loffler, 2012). These latter studies did argue for the global processing of RF4s with observer thresholds decreasing faster than predicted by probability summation as more modulation cycles were added to a single contour. However, those studies did generate probability summation estimates using high threshold theory (HTT), a method that Baldwin et al. (2016) and Kingdom, Baldwin, and Schmidtmann (2015) argue against. Although it must be noted that there were some differences in methodology between the studies using HTT and Baldwin et al. (2016) that are also quite likely to have influenced the results.

Baldwin et al. (2016) used fixed-phase (fixed orientation) stimuli for both the single-RF and quad-RF conditions, meaning the orientation of the pattern was the same between trials. They presented the stimuli in blocked trials (in which the observer would know how many cycles were being presented and in which location the maximum deformation would occur) or interleaved trials (in which, from trial to trial, the number of cycles was unknown and the orientation could be one of four known possibilities). When the stimulus presentation was blocked, Baldwin et al. (2016) found that thresholds were very similar to each other regardless of the numbers of cycles present. This is unsurprising as, with fixed phases, observers would know where deformation would be occurring in the pattern and would only need to monitor one location. Indeed it has been shown by Dickinson et al. (2012) that the presence of a known local cue (e.g., knowing where the deformation is going to occur) can result in stimuli being locally processed (poor integration), and the removal of the observer's certainty in the location of deformation restores this indication of global integration for RF patterns.

The interleaved presentations of both the quad- and single-RF conditions used by Baldwin et al. (2016) served to create spatial uncertainty in the location of deformation; however, this is not analogous to the random-phase (random orientation) presentation of an

RF pattern as the deformation could appear only at one of four locations. This meant the observers could monitor those four locations and disregard the remainder of the pattern, a strategy that favors local processing. This could explain why, for the single-RF condition, the integration slope obtained (−0.53) when fitting the improvement in threshold as a function of the number of modulation cycles was less than that found in Dickinson et al. (2012), who used random-phase RF4 stimuli and obtained an average integration slope of −0.80. The integration slope is the index of the power function that describes the relationship between threshold and number of cycles of modulation. Linear summation with constant noise results in a slope of −1; additive summation by the ideal observer in a two-interval task results in a slope of −0.50 (Tyler & Chen, 2000). Probability summation varies across observers but is typically between approximately −0.30 and −0.50 for HTT predictions (see appendix A of Baldwin et al., 2016) and between approximately −0.30 and −0.60 (Green, Dickinson, & Badcock, 2017) for signal detection theory (SDT) using random-phase RF patterns (depending on parameters used in the calculation, which is discussed below).

Although Baldwin et al. (2016) found that both the single-RF and quad-RF interleaved conditions produced similar integration slopes, the pattern of results for the two stimuli were different. As the number of modulated cycles increased for the single-RF condition, the thresholds for the blocked and interleaved presentations diverged from one another whereas increased cycles of modulation for the quad-RF condition resulted in the thresholds of the blocked and interleaved presentations converging. This difference in the pattern of results found for the two stimuli may suggest a difference in the way they are being processed by the visual system or perhaps the strategy adopted by the observers (see Green et al., 2017, for a discussion of the possible strategies adopted by the observers).

Previously, researchers investigating global processing of RF patterns have modeled probability summation estimates using HTT (Dickinson et al., 2015; Dickinson et al., 2012; Loffler et al., 2003; Schmidtmann et al., 2012; Tan et al., 2015; Tan et al., 2013); however, Baldwin et al. (2016) obtained receiver operating characteristics (ROC) curves to demonstrate that detection of RF patterns is better described by SDT than HTT and argued further that probability summation estimates should, therefore, be derived using the methods of SDT. We agree with them that the curved fit of SDT provided a better explanation for their ROC data than HTT and, therefore, also use SDT to generate probability summation estimates for RF patterns; however, HTT estimates are also included as a comparison to SDT to facilitate comparison with earlier studies.

Methods

Observers

Two of the authors and nine naïve observers participated in the current study. Participant ED has a divergent squint and used a black opaque occluder (eye patch) to cover his left eye during testing. All subjects had normal or corrected-to-normal visual acuity, which was assessed using a LogMAR chart. The research was approved by the University of Western Australia human research ethics committee and conforms to the Declaration of Helsinki. All participants gave informed written consent.

Stimuli

The stimuli were RF patterns (Loffler et al., 2003). An RF pattern has its radius modulated by the following formula:

$$R(\theta) = R_0 \times [1 + A\sin(\omega\theta + \varphi)], \quad (1)$$

where θ is the angle created with the x-axis, R_0 defines the mean radius (1° of visual angle in all conditions), A sets the amplitude of modulation (proportion of mean radius), ω refers to the frequency of modulation (number of cycles per 2π radians), and φ refers to the phase of the sinusoidal modulation that controls the rotation of the pattern (randomized for each pattern for each trial). A first derivative of a Gaussian (D1) was used to ensure a smooth transition between modulated and unmodulated sectors, replacing the first and last half cycles of the train of modulation as also employed by Loffler et al. (2003). Therefore, at one cycle, the modulated sector conforms solely to a D1 with a maximum slope and amplitude identical to that which would be produced by a sine wave (Loffler et al., 2003). The cross section of the luminance profile of the path conformed to a fourth derivative of a Gaussian (D4) with a frequency spectrum peaking at 8 c/deg (Loffler et al., 2003; Wilkinson et al., 1998), where $f_{peak} = \sqrt{2}/\pi\sigma$ (equation 2 from Wilkinson et al., 1998), resulting in a sigma (σ) of 3.376′ of visual angle.

Apparatus

Stimuli were generated using a PC (Pentium 4, 2.4 GHz; Intel, Santa Clara, CA) and custom software written in MATLAB 7.2.0 (MathWorks, Natick, MA). The observers viewed a CRT Sony Trinitron CPD-G420 monitor (100 Hz refresh rate; Sony Corp, Tokyo, Japan), which presented the stimuli from the frame buffer of a Cambridge Research Systems (CRS) VSG2/

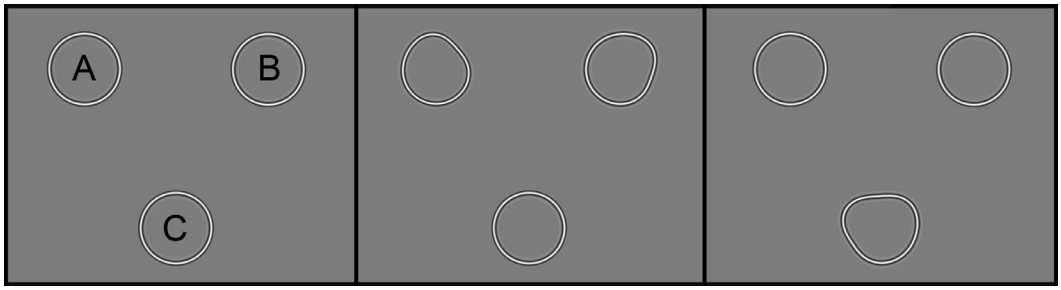

Figure 2. Three example stimulus presentations used in the experiment: left, a reference stimulus containing unmodulated circles ($A = 0$ in Equation 1; letters shown for illustrative purpose only and were not present for testing); middle, a test stimulus with an RF3(1) at locations A and B; and right, another test stimulus with an RF3(2) at location C. Both the right and middle stimuli contain two cycles of modulation; however, they are presented on one and two contours, respectively.

5 visual stimulus generator (CRS Ltd, Rochester, UK). Screen resolution was 1,024 × 768 pixels, and viewing distance was stabilized at a distance of 58.75 cm using a chin rest, which resulted in each pixel subtending a visual angle of 2′. An Optical OP 200-E photometer (head model number 265) and the CRS Desktop software (CRS Ltd, Rochester, UK) were used to linearize the luminance response and to calibrate background luminance to 45 cd/m^2 and maximum luminance to 90 cd/m^2, resulting in a Weber contrast of one. The minimum luminance was 17.14 cd/m^2, which resulted in a Michelson contrast of 0.68 for our stimuli. Responses were signaled using the left and right buttons of a mouse. Observers were instructed to fixate on a square (6′ side length) in the center of the screen where stimuli were presented with the center of the entire stimulus able to vary ±6′ of visual angle in the horizontal and vertical directions. This was done to reduce retinal afterimages to the luminance profile while maintaining the same spatial relationship between the individual RF patterns.

Procedure

A two-interval forced-choice paradigm was used with observers reporting which interval contained patterns most deformed from circular. One interval contained the reference stimulus, which consisted of three spatially separated circles ($A = 0$ in Equation 1). These circles were centered 3° of visual angle away from the center of the stimulus and had a radius of 1° of visual angle, and their centers were distributed to fixed locations around a circle and separated by an angle of 120° (see Figure 2). The other interval contained the test stimulus, using an identical layout to the reference stimulus with one or more RF patterns replacing one or more circles (depending on condition, explained below). The order of presentation was randomly determined for each trial, and both the reference stimulus and the test stimulus (i.e., all three contours) were jittered ±6′ of visual angle in the horizontal and vertical directions between trials; however, there was no movement of the circles relative to each other.

The current study investigated integration within RF patterns, i.e., when deformation is applied to a single contour, and across RF patterns, i.e., when deformation is applied to multiple spatially separate contours. Our methodology is different from Baldwin et al. (2016), who used RF4s and when testing across patterns used four locations. As described below, we interleaved the within and across presentations of one, two, and three cycles of modulation. At two cycles of modulation, there were six conditions interleaved, requiring 30 min of testing. To adequately interleave four locations using RF4s, an approximate 1-hr block would be required to test two cycles of modulation, which would likely result in significant observer fatigue. Therefore, we chose to use three spatial locations with RF3s as our test stimulus to reduce the number of trials presented in a single block, and these patterns also demonstrate the steepest integration slopes, allowing the greatest chance for global processing across patterns.

Every stimulus was presented for 160 ms with a 300-ms interstimulus interval as used in our previous similar studies employing RF patterns (Bell, Badcock, Wilson, & Wilkinson, 2007; Bell, Dickinson, & Badcock, 2008; Dickinson, Bell, & Badcock, 2013). Each condition was tested in three blocks. In the first condition (one cycle), an RF3(1), i.e., an RF3 with one cycle of modulation, was presented at location A, B, or C. There were 150 trials per location (450 total), and on each trial, the contour containing deformation was randomly selected. In the second condition (two cycles), either one RF3(2) would appear at A, B, or C or two RF3(1)s would appear at AB, AC, or BC (see Figure 2). Again, within a block there were 150 trials per location (900 total), and locations were randomized between trials. In the third condition (three cycles), an RF3(3) would appear at A, B, or C or three RF3(1)s would appear (one at each location, ABC). As with the previous

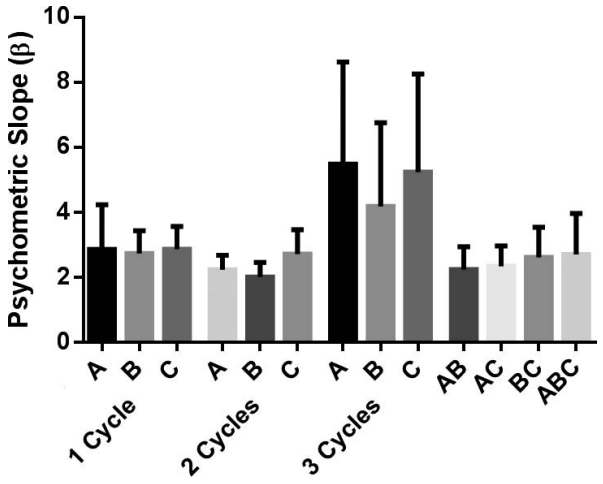

Figure 3. Average psychometric slopes with 95% confidence intervals for the different conditions.

conditions, 150 trials per location (600 total) and locations were randomized between trials. Data was collected using the ψ method (Kontsevich & Tyler, 1999), implemented using the Palamedes toolbox (Prins & Kingdom, 2009, available at http://www.palamedestoolbox.org), which optimized a Quick function (Quick, 1974; see Equation 2) with a λ value of 0.01. The parameters used in the slope estimation for the Ψ method incorrectly included values less than one. This resulted in a small number of the estimated psychometric slopes having values of less than one and, therefore, required reanalysis of the data using a weighted Quick function (as there was unequal sampling of stimulus intensities). This reanalysis resulted in no psychometric slope values less than one, and for this small number of psychometric functions, visual inspection suggested what R^2 values confirmed: the weighted Quick function provided a more accurate fit of the data (e.g., for observer AP, RF3(1) at location B, the weighted function resulted in $R^2 = 0.69$ compared with $R^2 = 0.36$ for the original fit). However, for the vast majority of data, there was no noticeable difference between the threshold and slope values obtained using the ψ method or the weighted Quick function, and therefore, this did not affect the experimental outcome.

Probability summation estimates were generated using procedures from both HTT and SDT to allow comparisons with earlier studies. Psychometric functions were plotted using a Quick function (Quick, 1974) with the formula

$$p(A) = 1 - 2^{-\left(1+(A/\alpha)^{\beta}\right)}, \quad (2)$$

where p is the probability of correct response, A is the amplitude of modulation as a proportion of the radius on an unmodulated circle, α is the amplitude producing the 75% correct response level (the threshold), and β controls the slope of the psychometric function. Under HTT (when probability summation is in operation) the slope of the line indicating the improvement in threshold as more cycles are added is estimated by $-1/\overline{\beta}$, where $\overline{\beta}$ is the average of the slopes of the psychometric functions for all cycles of the RF pattern. As can be seen in Figure 3, psychometric function slopes (β) did not decrease with increasing numbers of cycles of modulation contrary to probability summation estimates modeled using SDT (Pelli, 1985).

Following Baldwin et al. (2016), we estimated probability summation under SDT by calculating d' using the routine PAL_SDT_2AFC_PCtoDP from Prins and Kingdom (2009). These values were used along with stimulus intensity to solve the following equation with respect to g and τ:

$$d' = (gA)^{\tau}, \quad (3)$$

where d' is internal strength of a signal, g is a scaling factor incorporating the reciprocal of the internal noise standard deviation, A is the stimulus intensity, and τ is the exponent of the internal transducer (which controls the rate at which the observer is converting increased stimulus intensity to increased proportion of correct responses).

Under SDT, the percentage correct estimated for probability summation is given by (see Kingdom et al., 2015, for further details)

$$Pc = n \int_{-\infty}^{\infty} \phi(t-d')\Phi(t)^{QM-n}\Phi(t-d')^{n-1}dt + (Q-n)\int_{-\infty}^{\infty} \phi(t)\Phi(t)^{QM-n-1}\Phi(t-d')^{n}dt, \quad (4)$$

where Pc is the proportion correct and set at 0.75, t is sample stimulus strength (amplitude); the heights of the noise and signal distributions at t are given by $\phi(t)$ and $\phi(t-d')$, respectively. $\Phi(t)$ and $\Phi(t-d')$ are the areas under the noise and signal distributions less than t, Q is the number of monitored channels (defined below), M is the number of alternatives in the forced-choice task (two in the current study), and n is the number of stimulus components (discussed below). The fitting of this equation is also implemented in the Palamedes toolbox (for full details, see Prins & Kingdom, 2009, available at http://www.palamedestoolbox.org). As the stimuli used are random-phase RF patterns, the observer is always uncertain of the location of deformation, and therefore, we assume a fixed attention window (with which the number of channels is greater than the number of local elements; see Kingdom et al., 2015, for a detailed explanation of fixed attention window paradigms).

Results

Figure 4 shows the results for the within RF pattern conditions and the across RF patterns conditions (see Appendix A for individual observer plots). A 4 (A, B, C, across) × 3 (one, two, or three cycles) repeated-measures factorial ANOVA was used to examine the effect of condition and number of cycles on detection thresholds. There was a significant main effect of both condition, $F(3, 30) = 21.07$, $p < 0.001$, $\eta_p^2 = 0.68$, and number of cycles, $F(2, 20) = 157.31$, $p < 0.001$, $\eta_p^2 = 0.94$. There was also a significant interaction effect, $F(6, 60) = 5.63$, $p < 0.001$, $\eta_p^2 = 0.36$. Pair-wise comparisons revealed that thresholds for one cycle of modulation were significantly higher than two and three cycles of modulation ($ps < 0.05$), and two cycles of modulation was significantly higher than three cycles of modulation ($p < 0.05$), which was irrespective of condition.

Because of the interaction effect, three one-way repeated-measures ANOVAs were performed to examine the effect of condition for each cycle of modulation. There was no significant main effect of condition at one cycle of modulation, $F(3, 27) = 0.02$, $p = 0.99$, $\eta_p^2 = 0.002$. There was a significant main effect of condition at two cycles of modulation, $F(3, 30) = 14.73$, $p < 0.001$, $\eta_p^2 = 0.60$, with pair-wise comparisons revealing the across RF patterns condition had significantly higher thresholds than all three within RF pattern conditions ($ps < 0.05$). There was no significant difference between the three pattern locations for the within RF pattern conditions ($ps > 0.05$). At three cycles of modulation, there was also a significant main effect of condition, $F(3, 30) = 16.35$, $p < 0.001$, $\eta_p^2 = 0.62$, the across RF patterns condition had a significantly higher threshold than the three within RF pattern locations ($ps < 0.05$), and there was no significant difference between the thresholds of the three within RF pattern locations ($ps > 0.05$). It is clear from the analysis and Figure 4 that the amount of improvement in thresholds for the across RF patterns conditions is less than for the within RF patterns conditions with increasing number of cycles.

To determine whether there is any evidence of global processing, the slopes of the lines joining the thresholds were compared with the probability summation slopes predicted by both HTT and SDT. The HTT probability summation slope estimate was calculated by the simple formula described in the Methods for both within RF patterns and across RF patterns. Probability summation estimates under SDT were calculated for a high and low number of channels (Q). This method was used by Cribb et al. (2016), with which the number of stimulus components (n) is increased by one with each additional cycle of modulation added, and the number of channels (Q) was three for the "low" calculation and 120 for the "high" calculation. The number 120 is the

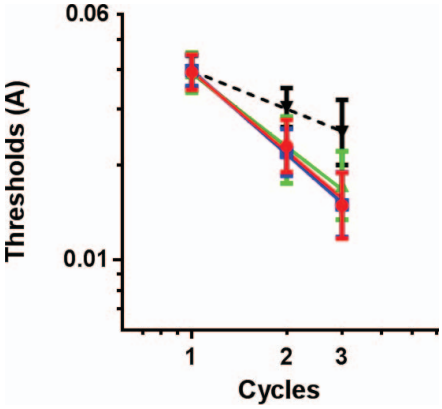

Figure 4. Geometric means of 11 observers with 95% confidence intervals for the within RF pattern conditions (red, location A; blue, location B; and green, location C) and the across RF patterns condition (black dashed line).

number of 1° rotations (out of 360°) an RF3 with three cycles of modulation could make before the pattern was repeated (see Green, Dickinson, & Badcock, in press). This was chosen as (a) the maximum difference in orientation (the zero-crossing of the sine wave, i.e., the difference between the pattern's tangent and a circle's tangent) is a very local feature that is detected first (Dickinson et al., 2012) in modulation detection tasks; (b) random-phase results in spatial uncertainty with regard to this feature; and (c) therefore, a large number of locations would need to be monitored assuming probability summation. This number is not critical to the current results, however, and is discussed in detail below.

As there are three RF patterns presented simultaneously, the number of channels the observer is required to monitor is obviously three times as great. Therefore, we will be using nine channels for our "low" SDT probability summation estimate and 360 channels for our "high" SDT probability summation estimate. Kingdom et al. (2015) demonstrated that increasing the number of channels increases observer thresholds and also has the resultant effect of decreasing probability summation slopes. Therefore, increasing the number of channels makes it easier to reject probability summation, and we believe that for three RF patterns in random phase 360 channels is an appropriate estimate. The nine-channel estimate is too conservative as it assumes one channel per cycle, which is only appropriate for fixed-phase patterns (Green et al., 2017), but we have included it for comparison as a lower limit.

Analysis of the observer thresholds found no significant difference between thresholds for the within RF pattern conditions (i.e., no difference in thresholds within a single contour at locations A, B, or C) but did find a significant difference in thresholds for the within RF pattern conditions compared with the across RF patterns condition. Therefore, analysis of the observer

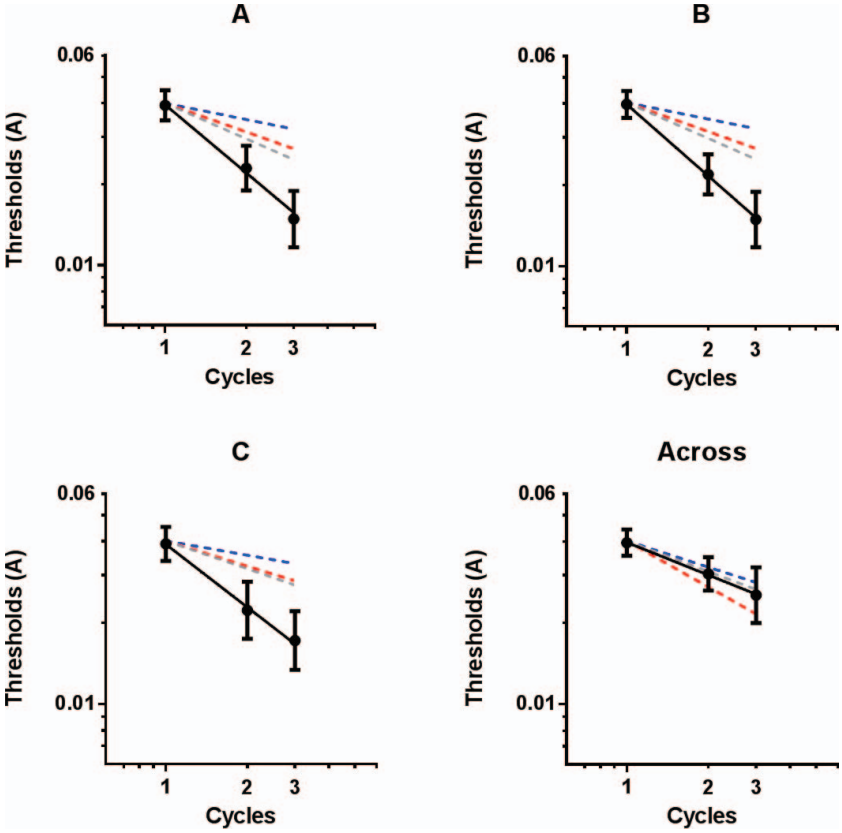

Figure 5. Geometric mean for 11 observers with 95% confidence intervals (CIs) for conditions A, B, C, and across patterns. Solid black lines show the integration slopes (−0.82, CI [−0.58, −1.07]; −0.84, CI [−0.62, −1.06]; −0.72, CI [−0.45, −0.99]; and −0.36, CI [−0.16, −0.57], respectively), and the dashed lines display the probability summation estimates (gray, HTT [−0.44, −0.43, −0.34, −0.38]; red, SDT 9 channels [−0.36, −0.36, −0.31, −0.57]; blue, SDT 360 channels [−0.20, −0.20, −0.18, −0.32] for [A, B, C, across], respectively).

slopes and their probability summation estimates will be split into within RF patterns and across RF patterns. Figure 5 displays the averaged observer thresholds for each of the four conditions along with the three probability summation estimates used to investigate global processing.

To examine the within RF pattern conditions, a 3 (A, B, C) × 4 (observer slope, HTT PS, SDT nine channels, SDT 360 channels) repeated-measures factorial ANOVA was used to examine the effect of location and model type on slope estimate. There was no significant main effect of location, $F(2, 20) = 2.98$, $p = 0.08$, $\eta_p^2 = 0.25$, and there was no significant interaction effect, $F(6, 60) = 0.28$, $p = 0.95$, $\eta_p^2 = 0.03$. However, there was a significant main effect of model type, $F(3, 30) = 58.35$, $p < 0.001$, $\eta_p^2 = 0.87$. Planned comparisons revealed observer slopes (estimates given in Figure 5 caption) were significantly steeper than all probability summation slope estimates from HTT and SDT ($ps < 0.05$).

A one-way repeated-measures ANOVA was used to examine the effect of model type on slope estimate for the across RF patterns condition. There was a significant main effect of model type, $F(3, 30) = 4.92$, $p = 0.007$, $\eta_p^2 = 0.33$, and pair-wise comparisons indicated there was a significant difference between the slopes of the SDT 9 and SDT 360 probability summation estimates ($p < 0.05$), but the observer slopes were not significantly different from any of the probability summation estimates from HTT or SDT ($ps > 0.05$).

Discussion

The purpose of the current paper was to examine the assertion that integration results reflect only local processing. This was done by distributing cycles of modulation either across multiple contours or around a single contour. The results demonstrate that, in our study, integration of information within a single RF pattern is significantly stronger than across RF patterns. There appeared to be no preference for the spatial location of the RF pattern as there was no consistent increased sensitivity in the lower visual field (a result differing from that of Schmidtmann, Logan, Kennedy, Gordon, & Loffler, 2015, which is discussed below). Comparison of observed thresholds and those

predicted by probability summation using both HTT and SDT showed strong evidence for the global processing within RF patterns but no evidence of global processing across RF patterns.

As originally noted by Loffler et al. (2003), when introducing the method of changing number of cycles for a given RF number, the use of fixed-phase RF patterns could potentially lead to localized attention with the observer concentrating on a fraction of the contour and disregarding global aspects. Dickinson et al. (2012) demonstrated that this can change the results substantially, and we believe this explains the difference between the current results and those of Baldwin et al. (2016). Our use of random-phase stimuli, coupled with uncertainty about whether the cycle(s) of modulation would appear on one pattern or distributed across them (within and across), meant the observer was unable to anticipate the location(s) of deformation. This required them to monitor the entire contour of each of the RF patterns and resulted in strong integration of information within discrete RF patterns but not across them. Baldwin et al. (2016) used fixed-phase stimuli, potentially introducing a highly salient local cue that resulted in decreased thresholds, particularly for the more difficult patterns to detect (one and two cycles of modulation), which would result in a shallower slope and, therefore, reduce the estimated strength of integration. The interleaving of conditions (one, two, three, and four cycles) in their study did not introduce enough spatial uncertainty as information could only appear in one of four possible locations. Therefore, observers were not required to monitor the whole pattern and were still able to use a local processing strategy.

Another potential explanation for the difference between the current results and those of Baldwin et al. (2016) is their 300-ms presentation time compared with the 160 ms of the current study. The increased duration in Baldwin et al. allows the observer to make a saccade during presentation. This, again, allows the observer to utilize different strategies, potentially moving the focal point to different parts of the contour in an attempt to get more information.

Within the pattern of results obtained by Baldwin et al. (2016), there is evidence for a difference in the processing of the single-RF condition compared with the quad-RF condition. They found a difference in thresholds at one cycle of modulation for the interleaved and blocked presentations of the quad-RF condition (see figure 6 of Baldwin et al., 2016). This difference decreased with more cycles of modulation until they converged at four cycles of modulation. This pattern of results is consistent with that described in Kingdom et al. (2015) for probability summation when using a fixed attention and matched attention window. This suggests the observer monitoring one location as there is no improvement in thresholds within the blocked condition when more cycles are added.

For the single-RF condition, the thresholds were the same at one cycle of modulation for the interleaved and blocked presentations, but they diverged with increasing cycles of modulation (Baldwin et al., 2016). This pattern of results cannot be explained using a probability summation model. At one cycle of modulation, probability summation would predict that the spatial uncertainty created by the interleaved presentation would result in higher observer thresholds than for the blocked presentation (this is what is evident from their quad condition). The thresholds for the interleaved condition start at the same threshold for one cycle of modulation and then decrease faster than for the blocked condition. This means the performance for the interleaved condition (in which the observer does not know the location of deformation) is better than for the blocked condition (in which the observer knows exactly where deformation will occur). No probability summation model can explain this result as they necessarily predict the interleaved presentation could never achieve thresholds less than the blocked presentation (Kingdom et al., 2015).

Therefore, for the interleaved presentation of the single-RF condition to have a higher sensitivity than the blocked presentation (Baldwin et al., 2016), there must have been integration of information around the contour. For the blocked presentation, the observers were able to monitor a single location, which could explain the lack of change in thresholds found. The spatial uncertainty created by the interleaved presentation of the single-RF condition likely caused the observer to monitor all four locations at which deformation could occur. This enabled the integration of information from the other locations, resulting in a decreased threshold relative to those found for their blocked presentation; however, this integration was not enough to reject probability summation estimates as observers could still narrow down where the deformation would occur (one of four possible locations). This created a local cue that interacted with the global cue to reduce the integration slope (see Green et al., 2017, in which they demonstrate the effect of fixed phase on integration slopes of an RF3).

Habak, Wilkinson, Zakher, and Wilson (2004) used "nested" RF patterns to examine the interaction between patterns. In their study, they created stimuli consisting of an RF pattern (target) with a suprathreshold RF pattern inner ring or outer ring or both. They were looking at the masking effect (decrease in sensitivity to the target) produced by the suprathreshold masking patterns. Among their results, they found that the interaction between patterns had little to no effect outside of approximately 1°. The current study had RF patterns of 1° radius, 3° from the central

fixation point, and spaced with a subtended polar angle of 120°. This resulted in the contours being approximately 0.8° apart at their closest point. This separation would suggest the RF patterns should have been able to interact with each other, so this is not a likely explanation for the lack of integration found between patterns (i.e., being on separate contours matters).

Observer slopes were compared with probability summation estimates from both HTT and SDT. Baldwin et al. (2016) examined ROC curves for both of their conditions. They found evidence to suggest that HTT is not appropriate for the analysis of RF patterns as the straight line fit to the ROC predicted by HTT was significantly worse than the curved fit predicted by SDT. Therefore, we did not include HTT as a competing model, but rather to connect previous research with current theory. The current results show HTT to provide a more conservative estimate than the high number of channels (360) SDT estimate, which is consistent with Green et al. (2017). This was replicated across all conditions and supports the suggestion of Green et al. (2017) that the previous studies finding evidence of global processing using HTT probability summation estimates would likely have reached the same conclusions using probability summation estimates modeled using SDT.

As outlined in the Methods section, we used two estimates of probability summation from SDT, one with nine channels (an overly conservative estimate but following the one channel per cycle used by Baldwin et al., 2016) and the other with 360 channels (a more appropriate estimate for random-phase patterns). Statistical analysis supports what is readily apparent from Figure 5, that observers' slopes for locations A, B, and C are significantly steeper than all probability summation estimates from both HTT and SDT, and the across RF patterns condition was not significantly steeper than any probability summation estimates. As can be seen in Figure 5, increasing the number of channels decreases the probability summation slope. Some researchers may argue that 360 channels is too many; however, we were able to reject probability summation at nine channels (which is certainly too low for three random-phase RF patterns) and, therefore, would be able to reject it at any number greater than nine.

Our results highlight not only the importance of using random-phase RF patterns, but also an appropriate number of channels when calculating probability summation estimates. Baldwin et al. (2016) used fixed-phase RF patterns in their experiment, so using the RF number for the number of channels was correct (i.e., number of channels was equal to four although this assumes the participant is monitoring all four channels rather than monitoring a single channel); however, this severely limits the sensitivity of the test for global integration, and what we have shown is this approach should not be taken for random-phase patterns. Random-phase patterns have spatial uncertainty in the location of deformation, and using the RF number for the number of channels will produce probability summation estimates, which are too conservative.

It was suggested by Baldwin et al. (2016) that RF3 patterns may be a special case in which integration occurs, and this might not occur for higher frequency RF patterns (i.e., RF4 and above). They cite the steep integration slopes (of the RF3) as evidence of their difference to other low-frequency RF patterns; however, this is unsurprising as it has been noted that the integration slopes for RF patterns decrease with increasing RF number (Loffler et al., 2003), so an RF3 would be expected to have steeper integration slopes than patterns with higher RF numbers (also see Green et al., in press). Dickinson et al. (2012) suggested that the difference in thresholds for differing RF patterns is actually a result of the use of amplitude of modulation rather than gradient at zero crossing as the measurement of threshold (see figure 7 of Dickinson et al., 2012). When they replotted results for three participants for an RF2, RF3, RF4, and RF6 using gradient at the zero crossing as a function of number of cycles of modulation, they found that thresholds across all four patterns were the same when they had the same number of cycles of modulation. This suggests that low-frequency RF patterns are processed in the same manner, and an RF3 is not a special case to be considered separate from other low-frequency patterns.

Observers were instructed to focus on the fixation point, and as the presentation times were 160 ms, we are confident in the RF patterns being presented in the upper and lower visual fields. As we found no significant difference in thresholds at locations A, B, or C, our results are also contrary to those found by Schmidtmann et al. (2015), who also used RF3s and found a lower field visual preference for RF patterns. In their study, they looked at thresholds for detection of straight lines, curves, and RF patterns. For straight lines and curves, they found no visual field preference (i.e., there was no difference in thresholds between the upper, lower, right, or left visual fields), but for RF patterns, they found a lower visual field advantage (i.e., thresholds for the lower visual field were significantly lower than for other areas). They note that previous studies have shown a lower visual field advantage for reaching and grasping (visuomotor) tasks (Danckert & Goodale, 2003; Previc, 1990; Rossit, McAdam, Mclean, Goodale, & Culham, 2013), cite this as a reason for their investigation of these simple shapes and components, and suggest this increased sensitivity in the lower visual field may be a result of the fact that humans typically manipulate objects in the lower visual field.

However, the results of Schmidtmann et al. (2015) are not consistent with those of Rossit et al. (2013) as, although they did find a lower visual field preference when grasping for objects, this result was not found for passively viewed objects. The results of Rossit et al. are consistent with the idea that action and perceptual pathways are different (Goodale & Milner, 1991; Goodale & Milner, 1992; Milner & Goodale, 2008) and, therefore, may have differing visual field biases (Danckert & Goodale, 2003). Additional evidence also comes from Wilkinson, Haque, Or, Gottlieb, and Wilson (2016), who also find no difference in sensitivity to motion-defined RF patterns when presented in either the upper or lower visual field. Although these patterns are defined by motion, the pattern of results for changes in frequency, radius, and cycles of modulation are highly similar to static RF patterns. This suggests a similarity in the processing of these two stimuli, which is supported by the results of Tanaka and Yotsumoto (2016), who found evidence that motion trajectories are being processed in the ventral visual stream (also see Green, Dickinson, & Badcock, 2018). Thus, the preference for lower visual field when grasping may not be the explanation for the results found by Schmidtmann et al. (2015), and it is clear that future research is required.

The results of the current study found evidence for the global processing within discrete RF patterns but not across them, suggesting it reflects the processing of object contours rather than the detection of replications of local features in an image. There was no evidence for any one of our eccentricity-matched locations resulting in greater sensitivity to deformation in shape. Our results are consistent with previous models of global shape processing of RF patterns (Poirier & Wilson, 2006) and biological data suggesting coding for the location of curvature maxima and minima relative to an object's center (Pasupathy & Connor, 2002).

Keywords: shape perception, global processing, signal detection theory, RF patterns, probability summation

Acknowledgments

The research was supported by Australian Research Council grants DP110104553 and DP160104211 to DRB and a UPA scholarship to RJG. Thanks to Alana Petersen, Alyse Withers, Clare Barry, Claire Gilchrist, Margaret Bowden, Payal Motiram Gurnani, Sophie Atkinson, Shannon Browning, Serena Cribb, Shannon O'Donnell, and Wei Jing Kok.

Commercial relationships: none.
Corresponding author: Robert J. Green.
Email: robert.green@research.uwa.edu.au.
Address: School of Psychological Science, The University of Western Australia, Perth, Australia.

References

Ariely, D. (2001). Seeing sets: Representation by statistical properties. *Psychological Science*, *12*(2), 157–162.

Badcock, D. R., Clifford, C. W., & Khuu, S. K. (2005). Interactions between luminance and contrast signals in global form detection. *Vision Research*, *45*(7), 881–889.

Baker, D. H., & Meese, T. S. (2011). Contrast integration over area is extensive: A three-stage model of spatial summation. *Journal of Vision*, *11*(14):14, 1–16, https://doi.org/10.1167/11.14.14. [PubMed] [Article]

Baldwin, A. S., Schmidtmann, G., Kingdom, F. A., & Hess, R. F. (2016). Rejecting probability summation for radial frequency patterns, not so Quick! *Vision Research*, *122*, 124–134, https://doi.org/10.1016/j.visres.2016.03.003.

Bell, J., & Badcock, D. R. (2008). Luminance and contrast cues are integrated in global shape detection with contours. *Vision Research*, *48*(21), 2336–2344, http://dx.doi.org/10.1016/j.visres.2008.07.015.

Bell, J., Badcock, D. R., Wilson, H., & Wilkinson, F. (2007). Detection of shape in radial frequency contours: Independence of local and global form information. *Vision Research*, *47*(11), 1518–1522.

Bell, J., Dickinson, J. E., & Badcock, D. R. (2008). Radial frequency adaptation suggests polar-based coding of local shape cues. *Vision Research*, *48*(21), 2293–2301.

Burr, D., & Ross, J. (2008). A visual sense of number. *Current Biology*, *18*(6), 425–428.

Cribb, S. J., Badcock, J. C., Maybery, M. T., & Badcock, D. R. (2016). Dissociation of local and global contributions to detection of shape with age. *Journal of Experimental Psychology: Human Perception and Performance*, *42*(11), 1761–1769, https://doi.org/10.1037/xhp0000257.

Danckert, J. A., & Goodale, M. A. (2003). Ups and downs in the visual control of action. In *Taking action: Cognitive neuroscience perspectives on intentional acts* (pp. 29–64). Cambridge, MA: MIT Press.

de Fockert, J., & Wolfenstein, C. (2009). Rapid extraction of mean identity from sets of faces. *The Quarterly Journal of Experimental Psychology*,

62(9), 1716–1722, https://doi.org/10.1080/17470210902811249.

Dickinson, J. E., & Badcock, D. R. (2007). Selectivity for coherence in polar orientation in human form vision. *Vision Research*, *47*(24), 3078–3087.

Dickinson, J. E., Bell, J., & Badcock, D. R. (2013). Near their thresholds for detection, shapes are discriminated by the angular separation of their corners. *PLoS One*, *8*(5), e66015, https://doi.org/10.1371/journal.pone.0066015.

Dickinson, J. E., Broderick, C., & Badcock, D. R. (2009). Selective attention contributes to global processing in vision. *Journal of Vision*, *9*(2):6, 1–8, https://doi.org/10.1167/9.2.6. [PubMed] [Article]

Dickinson, J. E., Cribb, S. J., Riddell, H., & Badcock, D. R. (2015). Tolerance for local and global differences in the integration of shape information. *Journal of Vision*, *15*(3):21, 1–24, https://doi.org/10.1167/15.3.21. [PubMed] [Article]

Dickinson, J. E., Han, L., Bell, J., & Badcock, D. R. (2010). Local motion effects on form in radial frequency patterns. *Journal of Vision*, *10*(3):20, 1–15, https://doi.org/10.1167/10.3.20. [PubMed] [Article]

Dickinson, J. E., McGinty, J., Webster, K. E., & Badcock, D. R. (2012). Further evidence that local cues to shape in RF patterns are integrated globally. *Journal of Vision*, *12*(12):16, 1–17, https://doi.org/10.1167/12.12.16. [PubMed] [Article]

Glass, L. (1969, August 9). Moire effect from random dots. *Nature*, *223*(5206), 578–580.

Glass, L., & Pérez, R. (1973, December 7). Perception of random dot interference patterns. *Nature*, *246*(5432): 360–362.

Goodale, M. A., & Milner, A. D. (1991, January 10). A neurological dissociation between perceiving objects and grasping them. *Nature*, *349*(6305), 154.

Goodale, M. A., & Milner, A. D. (1992). Separate visual pathways for perception and action. *Trends in Neurosciences*, *15*(1), 20–25.

Green, R. J., Dickinson, J. E., & Badcock, D. R. (2017). Global processing of random-phase radial frequency patterns but not modulated lines. *Journal of Vision*, *17*(9):18, 1–11, https://doi.org/10.1167/17.9.18. [PubMed] [Article]

Green, R. J., Dickinson, J. E., & Badcock, D. R. (in press). Convergent evidence for global processing of shape, *Journal of Vision*.

Green, R. J., Dickinson, J. E., & Badcock, D. R. (2018). The effect of spatio-temporal displacement on the integration of shape information, *Journal of Vision*, *18*(5):4, 1–18 https://doi.org/10.1167/18.5.4. [Article]

Habak, C., Wilkinson, F., Zakher, B., & Wilson, H. R. (2004). Curvature population coding for complex shapes in human vision. *Vision Research*, *44*(24), 2815–2823, http://dx.doi.org/10.1016/j.visres.2004.06.019.

Haberman, J., & Whitney, D. (2007). Rapid extraction of mean emotion and gender from sets of faces. *Current Biology*, *17*(17), R751–R753.

Haberman, J., & Whitney, D. (2009). Seeing the mean: Ensemble coding for sets of faces. *Journal of Experimental Psychology: Human Perception and Performance*, *35*(3), 718–734, https://doi.org/10.1037/a0013899.

Hess, R. F., Wang, Y.-Z., & Dakin, S. C. (1999). Are judgements of circularity local or global? *Vision Research*, *39*(26), 4354–4360.

Holmes, D. J., & Meese, T. S. (2004). Grating and plaid masks indicate linear summation in a contrast gain pool. *Journal of Vision*, *4*(12):7, 1080–1089, https://doi.org/10.1167/4.12.7. [PubMed] [Article]

Kingdom, F. A., Baldwin, A. S., & Schmidtmann, G. (2015). Modeling probability and additive summation for detection across multiple mechanisms under the assumptions of signal detection theory. *Journal of Vision*, *15*(5):1, 1–16, https://doi.org/10.1167/15.5.1. [PubMed] [Article]

Kontsevich, L. L., & Tyler, C. W. (1999). Bayesian adaptive estimation of psychometric slope and threshold. *Vision Research*, *39*(16), 2729–2737.

Loffler, G., Wilson, H. R., & Wilkinson, F. (2003). Local and global contributions to shape discrimination. *Vision Research*, *43*(5), 519–530.

McDougall, T. J., Dickinson, J. E., & Badcock, D. R. (2016). Larger receptive fields revealed using Battenberg stimuli to assess contrast summation with moving patterns. *Journal of Vision*, *16*(11):6, 1–17, https://doi.org/10.1167/16.11.6. [PubMed] [Article]

Meese, T. S. (2010). Spatially extensive summation of contrast energy is revealed by contrast detection of micro-pattern textures. *Journal of Vision*, *10*(8):14, 1–21, https://doi.org/10.1167/10.8.14. [PubMed] [Article]

Meese, T. S., & Hess, R. F. (2007). Anisotropy for spatial summation of elongated patches of grating: A tale of two tails. *Vision Research*, *47*(14), 1880–1892, http://dx.doi.org/10.1016/j.visres.2007.04.008.

Milner, A. D., & Goodale, M. A. (2008). Two visual

systems re-viewed. *Neuropsychologia*, *46*(3), 774–785.

Morrone, M., Burr, D. C., & Vaina, L. M. (1995, August 10). Two stages of visual processing for radial and circular motion. *Nature*, *376*(6540), 507–509.

Pasupathy, A., & Connor, C. E. (2002). Population coding of shape in area V4. *Nature Neuroscience*, *5*(12), 1332–1338.

Pelli, D. G. (1985). Uncertainty explains many aspects of visual contrast detection and discrimination. *Journal of the Optical Society of America A*, *2*(9), 1508–1532.

Persike, M., & Meinhardt, G. (2017). A new angle on contour integration: The role of corners. *Journal of Vision*, *17*(12):9, 1–13, https://doi.org/10.1167/17.12.9. [Article]

Poirier, F. J., & Wilson, H. R. (2006). A biologically plausible model of human radial frequency perception. *Vision Research*, *46*(15), 2443–2455.

Previc, F. H. (1990). Functional specialization in the lower and upper visual fields in humans: Its ecological origins and neurophysiological implications. *Behavioral and Brain Sciences*, *13*(3), 519–542.

Prins, N., & Kingdom, F. A. A. (2009). *Palamedes: Matlab routines for analyzing psychophysical data*. Retrieved from http://www.palamedestoolbox.org.

Quick, R. F. (1974). A vector-magnitude model of contrast detection. *Kybernetik*, *16*(2), 65–67, https://doi.org/10.1007/bf00271628.

Rossit, S., McAdam, T., Mclean, D. A., Goodale, M. A., & Culham, J. C. (2013). fMRI reveals a lower visual field preference for hand actions in human superior parieto-occipital cortex (SPOC) and precuneus. *Cortex*, *49*(9), 2525–2541.

Schmidtmann, G., Kennedy, G. J., Orbach, H. S., & Loffler, G. (2012). Non-linear global pooling in the discrimination of circular and non-circular shapes. *Vision Research*, *62*, 44–56.

Schmidtmann, G., Logan, A. J., Kennedy, G. J., Gordon, G. E., & Loffler, G. (2015). Distinct lower visual field preference for object shape. *Journal of Vision*, *15*(5):18, 1–15, https://doi.org/10.1167/15.5.18. [PubMed] [Article]

Tan, K. W., Bowden, V. K., Dickinson, J. E., & Badcock, D. R. (2015). Modulated textures with shape structures implied by a closed flow are processed globally. *Journal of Vision*, *15*(3):17, 1–18, https://doi.org/10.1167/15.3.17. [PubMed] [Article]

Tan, K. W., Dickinson, J. E., & Badcock, D. R. (2013). Detecting shape change: Characterizing the interaction between texture-defined and contour-defined borders. *Journal of Vision*, *13*(14):12, 1–16, https://doi.org/10.1167/13.14.12. [PubMed] [Article]

Tanaka, R., & Yotsumoto, Y. (2016). Networks extending across dorsal and ventral visual pathways correlate with trajectory perception. *Journal of Vision*, *16*(6):21, 1–14, https://doi.org/10.1167/16.6.21. [PubMed] [Article]

Tyler, C. W., & Chen, C.-C. (2000). Signal detection theory in the 2AFC paradigm: Attention, channel uncertainty and probability summation. *Vision Research*, *40*(22), 3121–3144.

Van Essen, D. C., Anderson, C. H., & Felleman, D. J. (1992, January 24). Information processing in the primate visual system: An integrated systems perspective. *Science*, *255*(5043), 419.

Vernon, R. J., Gouws, A. D., Lawrence, S. J., Wade, A. R., & Morland, A. B. (2016). Multivariate patterns in the human object-processing pathway reveal a shift from retinotopic to shape curvature representations in lateral occipital areas, LO-1 and LO-2. *Journal of Neuroscience*, *36*(21), 5763–5774.

Wilkinson, F., Haque, Y., Or, C. C.-F., Gottlieb, A. S., & Wilson, H. R. (2016). Detection of periodic motion trajectories: Effects of frequency and radius. *Journal of Vision*, *16*(7):10, 1–15, https://doi.org/10.1167/16.7.10. [PubMed] [Article]

Wilkinson, F., Wilson, H. R., & Habak, C. (1998). Detection and recognition of radial frequency patterns. *Vision Research*, *38*(22), 3555–3568, http://dx.doi.org/10.1016/S0042-6989(98)00039-X.

Appendix A. Individual observer results for all conditions

Figure A1 shows the individual observer thresholds for all conditions. There is some variation within the data, but critically, the pattern of results remains the same with similar performance at locations A, B, and C and reduced performance across RF patterns.

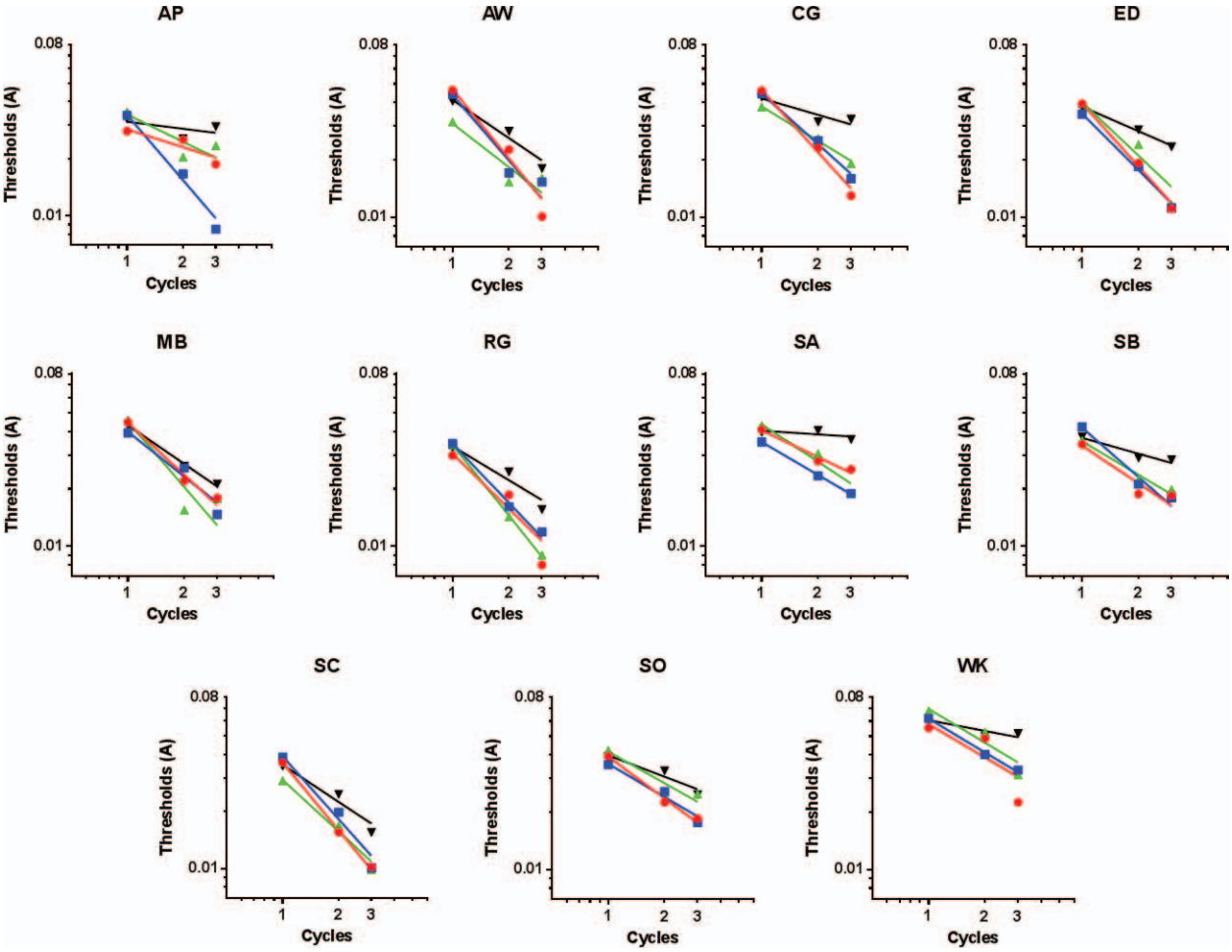

Figure A1. Individual observer thresholds for location A (red), B (blue), C (green), and across (black). The same pattern of results is apparent across observers with thresholds for across RF patterns higher than within RF patterns.